Ultrastructural anatomy of nodes of Ranvier in the peripheral nervous system as revealed by STED microscopy

Elisa D'Este[a,1], Dirk Kamin[a], Francisco Balzarotti[a], and Stefan W. Hell[a,1]

[a]Department of NanoBiophotonics, Max Planck Institute for Biophysical Chemistry, 37077 Goettingen, Germany

Contributed by Stefan W. Hell, November 28, 2016 (sent for review August 9, 2016; reviewed by Frank Bradke and Hjalmar Brismar)

We used stimulated emission depletion (STED) superresolution microscopy to analyze the nanoscale organization of 12 glial and axonal proteins at the nodes of Ranvier of teased sciatic nerve fibers. Cytoskeletal proteins of the axon (betaIV spectrin, ankyrin G) exhibit a high degree of one-dimensional longitudinal order at nodal gaps. In contrast, axonal and glial nodal adhesion molecules [neurofascin-186, neuron glial-related cell adhesion molecule (NrCAM)] can arrange in a more complex, 2D hexagonal-like lattice but still feature a ∼190-nm periodicity. Such a lattice-like organization is also found for glial actin. Sodium and potassium channels exhibit a one-dimensional periodicity, with the Na_v channels appearing to have a lower degree of organization. At paranodes, both axonal proteins (betaII spectrin, Caspr) and glial proteins (neurofascin-155, ankyrin B) form periodic quasi–one-dimensional arrangements, with a high degree of interdependence between the position of the axonal and the glial proteins. The results indicate the presence of mechanisms that finely align the cytoskeleton of the axon with the one of the Schwann cells, both at paranodal junctions (with myelin loops) and at nodal gaps (with microvilli). Taken together, our observations reveal the importance of the lateral organization of proteins at the nodes of Ranvier and pave the way for deeper investigations of the molecular ultrastructural mechanisms involved in action potential propagation, the formation of the nodes, axon–glia interactions, and demyelination diseases.

nodes of Ranvier | STED nanoscopy | cytoskeleton | axon–glia interaction | sciatic nerve

In recent years, knowledge of the ultrastructural organization of the axon initial segment (AIS) has been greatly extended by using optical nanoscopy to visualize its molecular composition. Stochastic optical reconstruction microscopy (STORM) and stimulated emission depletion (STED) microscopy were indeed crucial for the identification of a ∼190-nm periodic organization of the key components of the AIS. In particular, a periodic spatial arrangement was discovered for cytoskeletal proteins (actin, ankyrin G, betaIV spectrin), adhesion molecules (neurofascin), and channels (voltage-gated sodium Na_v channels) (1–4). In the distal part of the axon, this periodicity has been found for actin, adducin, ankyrin B, and betaII spectrin in virtually every neuron type from the central and peripheral nervous systems (CNS and PNS) (1, 2, 5, 6). Although myelination of axons does not alter the patterning of the subcortical cytoskeleton (5, 6), it changes its molecular composition, promoting the clustering of specific markers at the nodes of Ranvier, where the action potential is regenerated (reviewed in refs. 7, 8). At nodes of Ranvier, the myelin sheath formed by oligodendrocytes (in the CNS) or Schwann cells (in the PNS) is interrupted. Still, the nodal gap is surrounded by perinodal astrocytes and microvilli stemming from the Schwann cells in the CNS and PNS, respectively (9). Interestingly, the AIS and the nodes of Ranvier share most of their components, and at least two of them, ankyrin G and betaIV spectrin, are arranged in a periodic fashion in both compartments (3, 5).

The subcortical periodic cytoskeletal lattice is not a unique feature of neurons. Indeed, its periodic character was revealed also in oligodendrocyte precursors (5) and in Schwann cells (6). During axon ensheathment, cytoskeletal rearrangements—and actin disassembly in particular—constitute a fundamental process (10, 11). Altogether, these observations raise questions as to the relation and the possible reciprocal influence between the axonal and glial cytoskeletal lattices, especially at paranodes, which are the regions flanking the nodal gaps. There, the myelin loops contact the axon to form the paranodal junctions (PNJs), and the axon–glia interaction is extremely tight (12, 13). This interaction is also important for the recruitment of Na_v channels at nodal gaps of the PNS, as this process is orchestrated by proteins present on the membrane of the Schwann cells microvilli (14–17).

The molecular composition of nodes of Ranvier has been extensively studied in the last decades, however little is known about their molecular structure at the nanoscale. To gain insight into their organization and into the axon–glia interaction, we applied STED nanoscopy to analyze the ultrastructural molecular anatomy of the nodes of Ranvier in teased sciatic nerve fibers. We found a periodic organization of the axonal cytoskeletal proteins betaIV spectrin and ankyrin G and of potassium channels (K_v7.2 or KCNQ2) at nodal regions. Na_v channels and adhesion molecules (neurofascin-186, NrCAM) exhibited a less pronounced longitudinal periodicity. Predominantly glial proteins [actin, neuron glial-related cell adhesion molecule (NrCAM)] and neurofascin can form a 2D periodic structure with a hexagonal-like lattice. Interestingly, the distribution and geometry of proteins at the nodes is not always symmetrical and homogeneous. At paranodes, both axonal [betaII spectin and Contactin-associated protein

Significance

In vertebrates, the action potential travels along myelin-coated electrically isolated axons and is regenerated at the nodes of Ranvier, which lack myelination and are characterized by a tight interaction between the axon and glial cells. Specific sets of proteins are enriched in each region of the nodes. Thanks to its subdiffraction resolution, stimulated emission depletion (STED) microscopy here uncovers the organization of 12 of these proteins at the nanoscale. The superresolved imaging reveals an extremely fine interplay and alignment of the axonal and glial cytoskeleton, with a defined ∼190-nm periodicity. Furthermore, the results point to the importance of the lateral organization of proteins at nodal gaps, an aspect that is yet unexplored.

Author contributions: E.D., D.K., and S.W.H. designed research; E.D. performed research; E.D. and F.B. analyzed data; and E.D., D.K., F.B., and S.W.H. wrote the paper.

Reviewers: F.B., German Center for Neurodegenerative Diseases (DZNE); and H.B., Royal Institute of Technology.

Conflict of interest statement: S.W.H. is a founder of the companies Abberior GmbH and Abberior Instruments GmbH, commercializing fluorophores and microscope systems for superresolution applications, respectively.

Freely available online through the PNAS open access option.

[1]To whom correspondence may be addressed. Email: shell@gwdg.de or edeste@gwdg.de.

This article contains supporting information online at www.pnas.org/lookup/suppl/doi:10.1073/pnas.1619553114/-/DCSupplemental.

1 (Caspr)] and glial markers (neurofascin-155 and ankyrin B) are highly periodically arranged, with strictly related positions. Therefore, subdiffraction fluorescence microscopy of nodes of Ranvier indicates the presence of mechanisms that allow a fine alignment of the axonal and glial cytoskeleton and adhesion molecules.

Results

Nanoscale Organization of the Nodes of Ranvier.

Axonal cytoskeleton. We previously reported a periodic arrangement of the nodal-resident subcortical proteins betaIV spectrin and ankyrin G using STED nanoscopy on ∼300-nm thin sections of sciatic nerve fibers (3, 5). However, the 3D organization of the structure of interest is lost when slicing the specimen into thin sections. Therefore, we first aimed at imaging betaIV spectrin and ankyrin G in teased but unsliced sciatic nerve fibers (Fig. 1). Confocal microscopy demonstrated the successful antibody penetration and staining of the structures of interest throughout the sample (Fig. S1). The in situ STED analysis at enhanced lateral imaging resolution compared with diffraction-limited microscopy clearly visualized the ∼190-nm periodic arrangement of both proteins at nodes of Ranvier, even in intact nerve fibers and with conventional primary–secondary antibody labeling (Fig. 1 *A* and *B*, *Left*). Given the complex 3D geometry of unsliced sciatic nerve fibers and the small size of the nodes, we exploited the sensitivity of autocorrelation (AC) analysis to characterize the protein arrangements. AC provides information regarding the presence and orientation of a periodic organization. The peaks of a profile of the AC along a certain direction are related to the spacing, completeness, and stretch of the periodic structure. This analysis (*Materials and Methods*) proved to be extremely sensitive, as it is able to detect ordered molecules almost regardless of their concentration, even in cases where human assessments fail to readily recognize any periodicity (compare simulations shown in Figs. S2 and S3). AC on selected regions of the 3D betaIV spectrin and ankyrin G images revealed the presence of a predominantly longitudinal (i.e., along the axis of the axon) periodicity (Fig. 1 *A* and *B*, *Middle*), which becomes even more evident from a vertical line profile of the AC intensities (Fig. 1 *A* and *B*, *Right*). Indeed, the peaks show a regular periodicity. Interpeak spacings of several nodes of Ranvier were measured to better define this periodicity. Intensity line profiles traced on the raw STED images provided an average interpeak spacing of 188 ± 45 nm for betaIV spectrin (n_{nodes} = 35, $n_{spacings}$ = 205, ±1 SD for all spacings stated in this article) and 180 ± 59 nm for ankyrin G (n_{nodes} = 12, $n_{spacings}$ = 55) (Fig. 1*H*). These values are in agreement with our previously reported observations in thin sections (180 ± 35 nm for betaIV spectrin) (3, 5) and therefore indicate that STED nanoscopy is capable of revealing the ultrastructural organization at myelin sheath gaps even in intact fibers.

Na_v and K_v channels. Na_v channels are periodically arranged along the AIS (1, 4), colocalizing with ankyrin G. Because clustering of Na_v channels at nodes of Ranvier is required for action potential propagation, we analyzed their ultrastructural anatomy at the nodal gap. To our surprise, the periodicity of Na_v channels is not sharply one-dimensional (Fig. 1*C* and Fig. S4*A*). Indeed, besides the one-dimensional longitudinal component (Fig. 1*C*, *Left*), the AC often reveals also other directions of periodicity, and in some cases, the vertical line profile of the AC exhibits only few peaks at the expected distance (Fig. 1*C*, *Right*). Despite this, the interpeak spacing of the lattice-like structure was measured to be similar to that of the one-dimensional organization, at 192 ± 54 nm (n_{nodes} = 45, $n_{spacings}$ = 250) (Fig. 1*H*).

We then looked at potassium channels to understand if this behavior is a general feature of nodal channels or whether it is peculiar of Na_v channels. Specifically, we focused on the subunit K_v7.2 (KCNQ2), which is highly enriched at the nodes of the PNS along with K_v7.3 (KCNQ3) (18, 19). Immunolabeling of K_v7.2 in sciatic nerves indicates a sharp, one-dimensional periodicity (193 ± 31 nm, n_{nodes} = 44, $n_{spacings}$ = 243) (Fig. 1 *D* and *H* and Fig. S4*B*). Two-color stainings indicate that K_v7.2 interleaves with ankyrin G and Na_v channels, with their AC revealing the same period. However, the cross-correlation analysis (a measure of similarity of two series as a function of the lag of one relative to the other; see also Fig. S3) highlights a phase shift, indicating that Kv7.2 is spatially separated from sodium channels and ankyrin G at the nodes (Fig. S5). In conclusion, both Na_v and K_v channels are periodically arranged at the nodal gap, but the latter exhibits a more prominent longitudinal organization.

Adhesion molecules and glial proteins. We further studied the nanoarchitecture of the adhesion molecules neurofascin and NrCAM. Although the former is an axonal protein, the latter is present both in the axon and in the Schwann cell microvilli that surround the nodal gap (15). Neurofascin and NrCAM are enriched in the AIS, where they exhibit a weak periodic organization and intercalate with the actin lattice (3) (Fig. S6). Neurofascin was detected using an anti–pan-neurofascin antibody against the C terminus of the protein, and therefore, both nodes (where neurofascin-186 is present) and paranodes (with neurofascin-155) are stained in the corresponding images (Fig. 1*E*) (20). At the nodes, both neurofascin and NrCAM show two organizational features: a mainly longitudinal organization (Fig. 1 *E* and *F*, *Left*) and a 2D lattice-like pattern with several axes of periodicity, which appears as a hexagon in the AC and resembles the Na_v channel pattern (Fig. 1 *E* and *F*, *Right* and Fig. S2). Interestingly, actin also exhibits a similar arrangement at nodal gaps. Indeed, it forms complex filamentous periodic structures (Fig. 1*G*, *Left*), which, however, can also be as simple as single spots at the corners of hexagons (Fig. 1*G*, *Right*). When performing costainings with axonal markers, actin appears more on the outside of the axon, and therefore, we conclude that the strong actin signal at nodal gaps originates from glial actin present in the microvilli (Fig. S7). A vertical line profile on the AC of the hexagonal-like lattices generates peaks with an unexpected periodicity of ∼300 nm (compare with Fig. S2). Nevertheless, the ∼190-nm frequency sharply appears for all proteins by simply aligning the line profile with the nodes of the lattice (Fig. 1*G*, *Right*, gray line). In general, the interpeak spacings of neurofascin, NrCAM, and actin are similar to the other nodal proteins analyzed, with 200 ± 58 nm for neurofascin-186 (n_{nodes} = 62, $n_{spacings}$ = 238), 192 ± 62 nm for NrCAM (n_{nodes} = 20, $n_{spacings}$ = 120), and 182 ± 38 nm for actin (n_{nodes} = 37, $n_{spacings}$ = 186) (Fig. 1*H*). Axonal adhesion proteins, as well as proteins present on the Schwann cells microvilli, are thus found to be preferentially periodically organized at myelin sheath gaps.

Symmetry of the nodes. In some cases, nanoscopy revealed an inhomogeneous staining of nodal gaps, which was especially obvious in the case of Na_v channels. In 62 out of 137 nodes (45.2%), Na_v channels showed a longitudinal enrichment on lines, often accompanied by grooves with a less bright staining (Fig. S4*A*). These features can be asymmetrically distributed, as they appear only on one side of the node (i.e., on the upper or lower part). For the other analyzed proteins, the presence of lines and furrows is less prominent and more difficult to detect and quantify. Nevertheless, costaining of Na_v channels with K_v7.2 or neurofascin indicates overlapping patterns, with grooves almost depleted from or lines enriched with both proteins (Fig. S4 *C* and *D*), suggesting that these structures might be particular membrane folds. Another interesting nanoanatomical feature when imaging the two opposite sides of the nodes is the difference in the geometry of the sharp arrangement of the K_v7.2 lattice. Indeed, even if the pattern is one-dimensional and perpendicular to the axon on one side of the node, on the other side the lattice can appear distorted or tilted (Fig. S4*B*). Altogether, even if we cannot rule out that these differing patterns are caused by the sample preparation procedure, the observations suggest that nodal gaps are not necessarily symmetrical objects

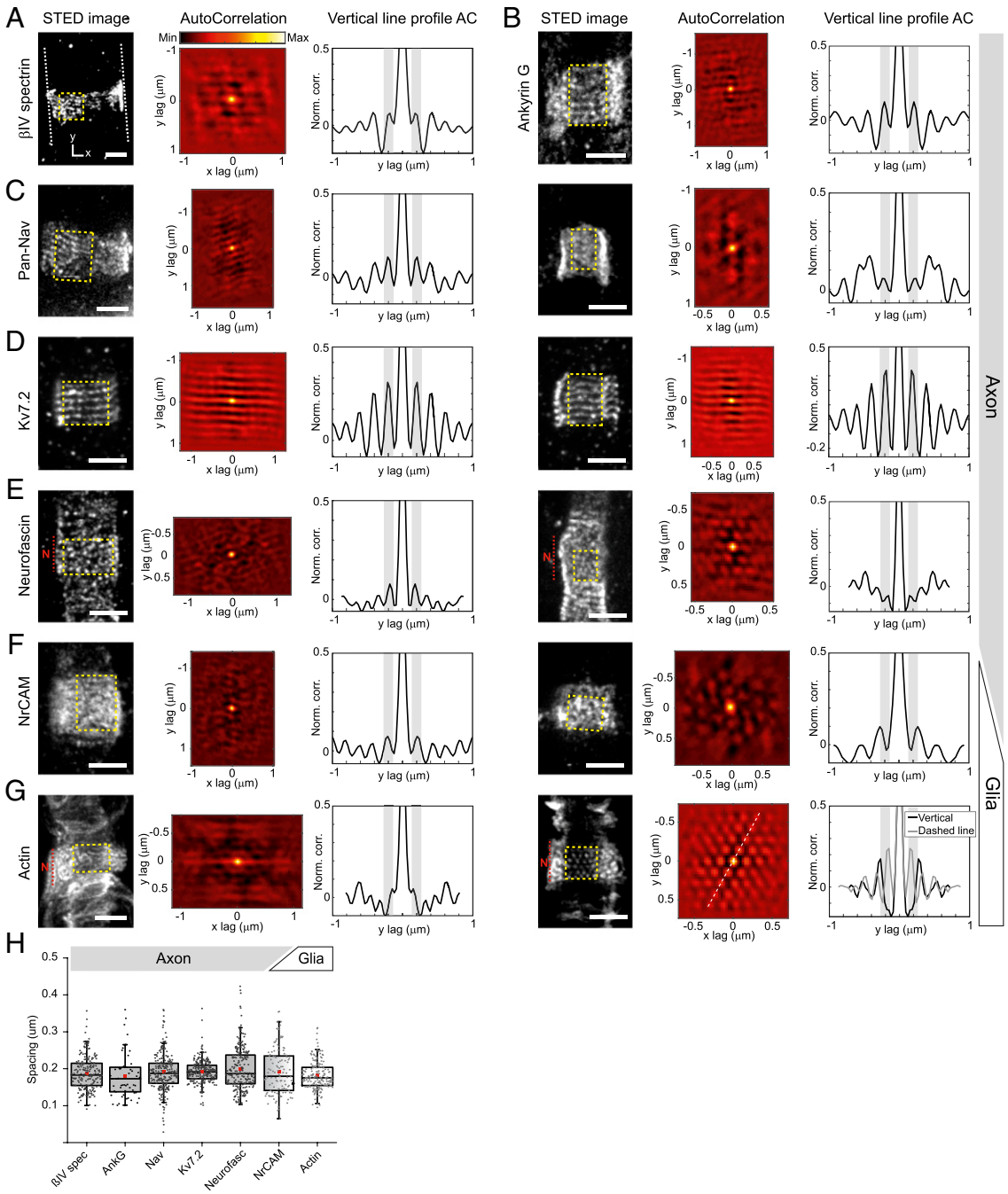

Fig. 1. Organization of proteins at nodal gaps of sciatic nerve fibers. Representative STED images (*Left*) are shown for each protein. The yellow dashed box on the STED image indicates the region in which the 2D AC (*Middle*) was performed. The *y* axis of the AC is aligned with the axon. AC intensities are depicted using a red hot look-up table. The vertical line profile AC (*Right*) is the plot line profile of intensities along a vertical 1-pixel wide line passing through the center of the AC and hence highlights the presence of longitudinal patterns. The gray bars are centered at ±0.2 μm *y* lag, where the peaks of periodicity are expected. (*A*) Representative image of axonal betaIV spectrin along with AC and line profile of the AC reveals a predominantly longitudinal periodicity. The dashed white lines indicate the outline of the axon, which has the same orientation in all other panels/proteins. (*B*) Axonal ankyrin G (monoclonal antibody) shows a predominantly longitudinal periodicity. Comparable results were obtained with both anti-ankyrin G antibodies used in this study. (*C*) Axonal voltage-gated sodium channels (Pan-Na_v) exhibit longitudinal periodic AC peaks at ∼190 nm (*Left*) or multiple, hexagonal-like axes of periodicity (*Right*). More examples of Na_v arrangements at the nodes are provided in Fig. S4*A*. (*D*) Subunit 7.2 of axonal voltage-gated potassium channel (K_v7.2 or KCNQ2, N terminus antibody) forms a highly periodic one-dimensional lattice. The two images represent opposing sides of the same node. More examples of K_v7.2 arrangements at the nodes are provided in Fig. S4*B*. Comparable results were obtained with both anti- K_v7.2 antibodies used in this study. (*E*) Axonal neurofascin has a ∼190-nm periodic organization but lacks a sharp longitudinal pattern. Neurofascin was detected using a pan-neurofascin antibody; therefore, paranodes are also stained. The red dashed line indicates the position of the node ("N"). (*F*) Axo-glial NrCAM shows either a mainly longitudinal ∼190 nm periodicity (*Left*) or a hexagonal-like pattern (*Right*), although with slightly longer spacing. (*G*) Glial actin exhibits a hexagonal-like periodic organization. The intensities along the dashed line on the right AC are represented in the vertical line profile AC (gray line). Note, even if actin is present both on the axon and in the microvilli, the signal is mainly produced by glial actin. The red dashed line indicates the position of the node ("N"). (*H*) Interpeak spacing of line profiles measured from the raw STED images. The box plot includes the 25th, 50th, and 75th percentile, whereas the whiskers indicate the SD. The red dots represent the average values. The periodicity of all proteins is within the same range of 180–200 nm. All image data were smoothed with a 1-pixel low pass Gaussian filter and represents the overlay of several optical sections. (All scale bars, 1 μm.)

but might have some folds in the membrane and that their spatial organization on opposing sides should be considered.

Axon–glia interaction at nodal gaps. The proteins present on the microvilli play a key role in the ultrastructural organization of the nodes (15–17, 21), and hence, a strong relation between the spatial arrangements of glial and axonal proteins can be hypothesized. To examine this, we performed dual-color STED recordings of the microvilli by labeling actin and the axon by staining the adhesion molecule neurofascin-186 (Fig. S7). Unfortunately, the sample preparation required for staining actin with phalloidin is not optimal for neurofascin-186, thus resulting in an incomplete labeling of the latter. As a result, ACs exhibit only one peak at ∼190 nm. The cross-correlation shows a weak out-of-phase periodicity, and neurofascin-186 puncta appear to be present in actin-deprived regions, suggesting a bias in the position of both proteins (Fig. S7).

In conclusion, although the proteins of the axonal cytoskeleton, betaIV spectrin and ankyrin G, show a pronounced longitudinal periodicity at nodal gaps, some axonal transmembrane proteins (K_v channels) follow this longitudinal periodicity, whereas others (Na_v channels, neurofascin-186, and NrCAM) are arranged in a more complex lattice, which also still features the ∼190-nm periodicity. This different arrangement could be due to the interaction with the Schwann cell microvilli, whose proteins (actin and NrCAM) can exhibit a hexagonal lattice-like order.

Nanoscale Organization of the Paranodes.

Axonal and glial markers. The ultrastructural organization of PNJs has been extensively investigated with electron microscopy and revealed the septate-like junctions (for example, refs. 12, 13, 22), but the arrangement of the main paranodal markers at the nanoscale is still unknown. We first analyzed the subcortical axonal cytoskeleton at paranodes by imaging betaII spectrin. BetaII spectrin shows a marked long-range longitudinal periodicity at paranodes, which extends to juxtaparanodes and internodes (5) and is also revealed by the AC (Fig. 2*A*). The interpeak spacing for betaII spectrin was measured to be 193 ± 32 nm ($n_{paranodes}$ = 37, $n_{spacings}$ = 247) (Fig. 2*E*) and is therefore consistent with the typical ∼190-nm lattice. Costaining and dual-color STED imaging of the nodal betaIV spectrin and the paranodal betaII spectin isoforms reveals a continuity of the spectrin scaffold along the axon, without any interruption at the transition between these two regions (Fig. S8).

Next, we investigated the arrangement of transmembrane proteins at the paranodes. We intended to find out if the periodic longitudinal organization of the subcortical cytoskeleton is preserved or partially transformed into a lattice, as shown for the nodes. STED nanoscopy of the axonal adhesion molecule Caspr at paranodes reveals a longitudinal periodic arrangement (Fig. 2*B*), with an interpeak spacing of 191 ± 53 nm ($n_{paranodes}$ = 63, $n_{spacings}$ = 305) (Fig. 2*E*). Likewise, the glial adhesion molecule neurofascin-155 features the presence of a highly periodic structure with an interpeak spacing of 206 ± 59 nm ($n_{paranodes}$ = 35, $n_{spacings}$ = 150) (Fig. 2 *C* and *E*). Finally, to prove the periodic organization of the glial cytoskeleton at paranodes, we analyzed ankyrin B, which is supposed to be present at myelin loops and to anchor neurofascin-155 at this position (23). Similar to the other paranodal proteins, ankyrin B is also organized in a periodic fashion (183 ± 34 nm, $n_{paranodes}$ = 34, $n_{spacings}$ = 140) (Fig. 2 *D* and *E*). The lattice formed by ankyrin B at paranodal loops, however, might be organized differently compared with the axonal ankyrin scaffold. Ankyrin B obviously cannot form a continuous subcortical lattice throughout the paranodes, as the myelin loops constitute separate cellular compartments, which necessarily interrupt the structure.

Relative arrangement of glial paranodal markers. To obtain additional insight into the arrangement of glial proteins at the paranodal loops and clarify their mutual localization, we performed dual-color STED nanoscopy of actin and the adhesion protein neurofascin-155. At paranodes, actin forms prominent fibers that surround the axon (5). Costaining of actin and neurofascin-155 indicates that the two proteins intercalate, similarly to the arrangement at the AIS and at the nodal gap. Indeed, even if the ACs of both species have a strong longitudinal periodicity, the cross-correlation reveals a prominent phase shift (Fig. 3 *A*, *C*, and *E*). This observation, together with the fact that the actin staining appears on the outside of neurofascin-155, suggests that the actin filaments are actually positioned not at the utmost tip of the paranodal loops but deeper inside or next to the membrane of the loops themselves. At the same time, ankyrin B and

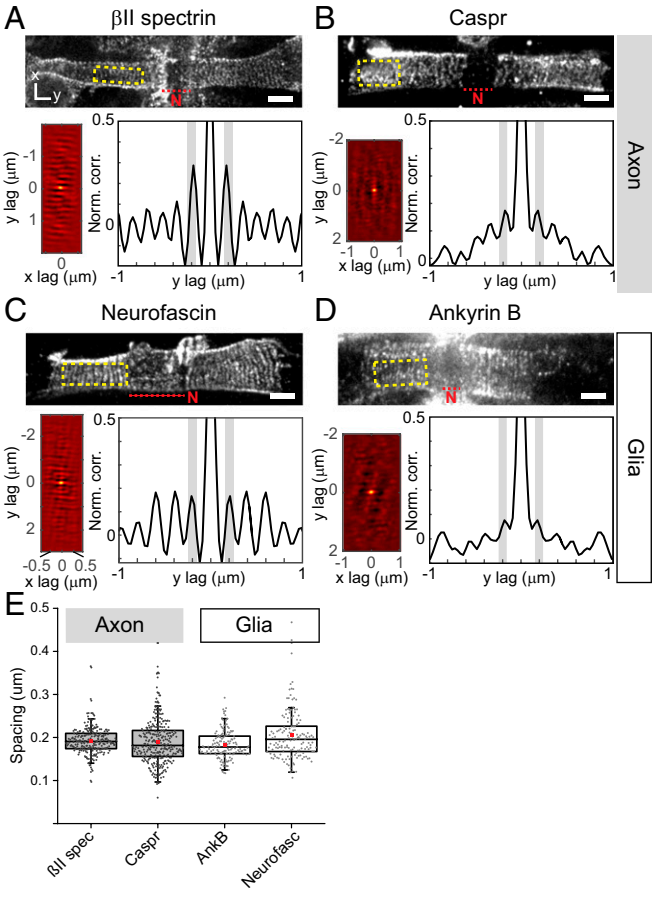

Fig. 2. Organization of proteins at paranodes of sciatic nerve fibers. Representative STED images of proteins at the paranodes (*Upper*). The red dashed line indicates the position of the node ("N"). The yellow dashed box on the STED image marks the region in which the AC was performed (*Lower Left*). The *y* axis of the AC is always aligned with the axon. (*Lower Right*) The plot line profiles of intensities along a vertical 1-pixel wide line passing through the center of the AC, highlighting the presence of longitudinal patterns. The gray bars are positioned at ±0.2 μm *y* lag, where the peaks of periodicity are expected. (*A*) Axonal betaII spectrin, (*B*) axonal Caspr, (*C*) glial neurofascin-155, and (*D*) glial ankyrin B (monoclonal antibody) all show a long-range ∼190-nm longitudinal periodic arrangement. The high background makes the ankyrin B pattern less pronounced but still discernable (see also Fig. 3 *B*, *D*, and *F*). Comparable results were obtained with both anti-ankyrin B antibodies used in this study. In *C* neurofascin was detected using a pan-neurofascin antibody; therefore, the node is also stained. (*E*) Interpeak spacing of line profiles measured on raw STED images. The box plot includes the 25th, 50th, and 75th percentile, whereas the whiskers indicate the SD. The red dots represent the average values. The periodicity of all proteins is within the same range of 180–206 nm. All image data were smoothed with a 1-pixel low-pass Gaussian filter and represent the overlay of several optical sections. (All scale bars, 1 μm.)

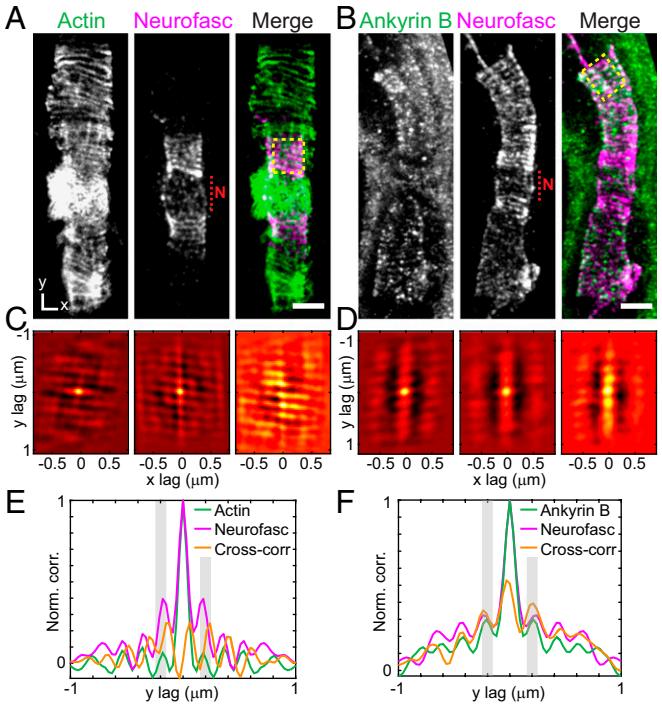

Fig. 3. Correlation between the glial proteins at paranodes. Two-color STED images of a node and paranodes in which (*A*) actin and neurofascin or (*B*) ankyrin B (monoclonal antibody) and neurofascin have been labeled. Single color images and overlay are shown. In *A*, neurofascin labeling is incomplete and only the part close to the node was stained. The nodal gap from the same image is depicted in Fig. S7. The red dashed line indicates the position of the node ("N"). (*C* and *D*) AC (for single-channel images) and cross-correlation (CC, for the merged image) of the regions indicated by the yellow dashed boxes in *A* and *B* reveal periodic longitudinal patterns for both AC and CC. The *y* axis is aligned with the axon. (*E* and *F*) Vertical line profiles of intensities along the panels shown in *C* and *D* confirm the ∼200-nm periodic organization of the glial proteins (gray bars positioned at ±0.2 μm *y* lag) and reveal an out-of-phase (for actin and neurofascin-155) or in-phase (for ankyrin B and neurofascin-155) cross-correlation. All image data were smoothed with a 1-pixel low-pass Gaussian filter and represent the overlay of several optical sections. (All scale bars, 1 μm.)

neurofascin-155 colocalize: The AC shows the same periodicity, and the cross-correlation confirms the alignment of the two proteins (Fig. 3 *B*, *D*, and *F*) (23).

Alignment of the axonal and glial cytoskeleton at paranodes. Given the presence of a periodic arrangement on both cellular sides of the paranodes, we investigated whether the structures are actually coaligned and if there is a correlation between the components of the axon and glia. To this end, we performed a set of dual-color STED recordings by colabeling an axonal and a glial protein. We started by costaining Caspr and neurofascin-155, which are supposed to interact through contactin (24). As shown in Fig. 4 *A*, *D*, and *G*, the proteins colocalize along transversal loops, feature the same periodicity, and their positions are strongly correlated, therefore confirming the biochemical and functional data from literature (20, 24–27).

We also looked at the positioning of the myelin loops with respect to the subcortical cytoskeleton of the axon by analyzing the relative localization of neurofascin-155 and betaII spectrin. The AC shows that the two protein patterns have the same periodicity. However, their positions are slightly shifted but not entirely complementary to each other, even if strongly cross-correlated (Fig. 4 *B*, *E*, and *H*). This result depends on the epitope recognized by the antibodies: The neurofascin antibody is directed against the short intracellular domain of neurofascin-155, whereas the betaII spectrin antibody binds to the C terminus of the protein. Spectrin tetramers are ∼200 nm long, run parallel to the cell membrane, and are formed by dimers that are connected head-to-head through their C termini, whereas the N terminus binds actin (28). Therefore, using antibodies directed against the N terminus of spectrin would generate a larger phase shift. Nevertheless, the results indicate the alignment of the myelin loops to the subcortical axonal cytoskeleton.

Additionally, we probed the correlation between the subcortical cytoskeleton of axon and glia by imaging betaII spectrin and ankyrin B. Once again, auto- and cross-correlation indicate the same in-phase periodicity of the proteins (Fig. 4 *C*, *F*, and *I*). The dual-color experiments therefore clearly indicate the alignment of the glial and axonal subcortical cytoskeleton. Taken together, both axonal and glial cytoskeletal proteins exhibit an almost one-dimensional longitudinal periodicity of ∼190 nm at paranodes. This organization is unperturbed up to the level of transmembrane proteins and likely reflects the organization of the myelin loops and PNJ.

Potassium channels at juxtaparanodes. Juxtaparanodal regions are found beneath the compact myelin next to the paranodes and are populated by different subtypes of voltage-gated potassium channel 1 (K_v1 channels), whose function is to stabilize the action potential conduction (29, 30). In cultured hippocampal neurons, the subtype $K_v1.2$ channels are located along the AIS; have a sharp, long-range periodic organization; and are aligned with actin, as evident from the cross-correlation (Fig. S6 *B*, *D*, and *F*). Because Na_v channels alternate with actin (1), $K_v1.2$ channels and Na_v channels are also interleaved along the AIS. In sciatic nerves, a periodic organization of $K_v1.2$ at juxtaparanodes is not visible (Fig. S9), even if the betaII spectrin scaffold is still periodically organized (Fig. 2*A* and Fig. 4*B*). Costaining of $K_v1.2$ and neurofascin shows a perfect complementarity of the two proteins at the transition between paranodes (with neurofascin-155) and juxtaparanodes, providing visual evidence of the function of the PNJ in keeping juxtaparanodal K_v channels separated from nodal Na_v channels (31, 32) (Fig. S9).

We thus observe that the subcortical axonal cytoskeletal organization at juxtaparanodes is not passed outwards to the $K_v1.2$ channels, whose localization is nevertheless influenced by the glial proteins.

Discussion

Nodes of Ranvier mediate saltatory conduction of the action potential and have been shown to be critical in the pathogenesis of various neurodegenerative diseases (33–36). Even if their molecular inventory has been well characterized, the organization of these molecules at the nanoscale is still largely unknown. We found that, at paranodes, cytoskeletal and adhesion molecules of both the axon and glia show a ∼190-nm longitudinal periodic arrangement and are coaligned, suggesting a role of the subcortical cytoskeleton in the arrangement of the PNJ (Fig. 5). Although axonal cytoskeletal proteins and K_v channels exhibit a longitudinal periodic order at the nodes, Na_v channels and glial proteins can be positioned in a more complex 2D lattice that resembles the one found in red blood cells (28). Microvilli of the Schwann cells orchestrate the positioning of the axonal transmembrane proteins at nodes (15–17, 21), which, at the same time, are subjected to the structure of the axonal subcortical cytoskeleton. Therefore, we propose a model in which the subcortical cytoskeletal proteins actin, spectrin, and ankyrin act as a scaffold onto which transmembrane proteins can be docked at discrete positions, which, in turn, might have an effect on the molecular anatomy of the microvilli. The actual localization of the transmembrane proteins likely depends on the positioning of both the axonal cytoskeleton and glial proteins (Fig. 5). In the CNS, the myelin sheath gaps are surrounded by the perinodal astrocytes (37), and the mechanism leading to the formation of the nodes of Ranvier differs from the one in the PNS presented here; indeed, it does not rely on the interaction with proteins present on the mi-

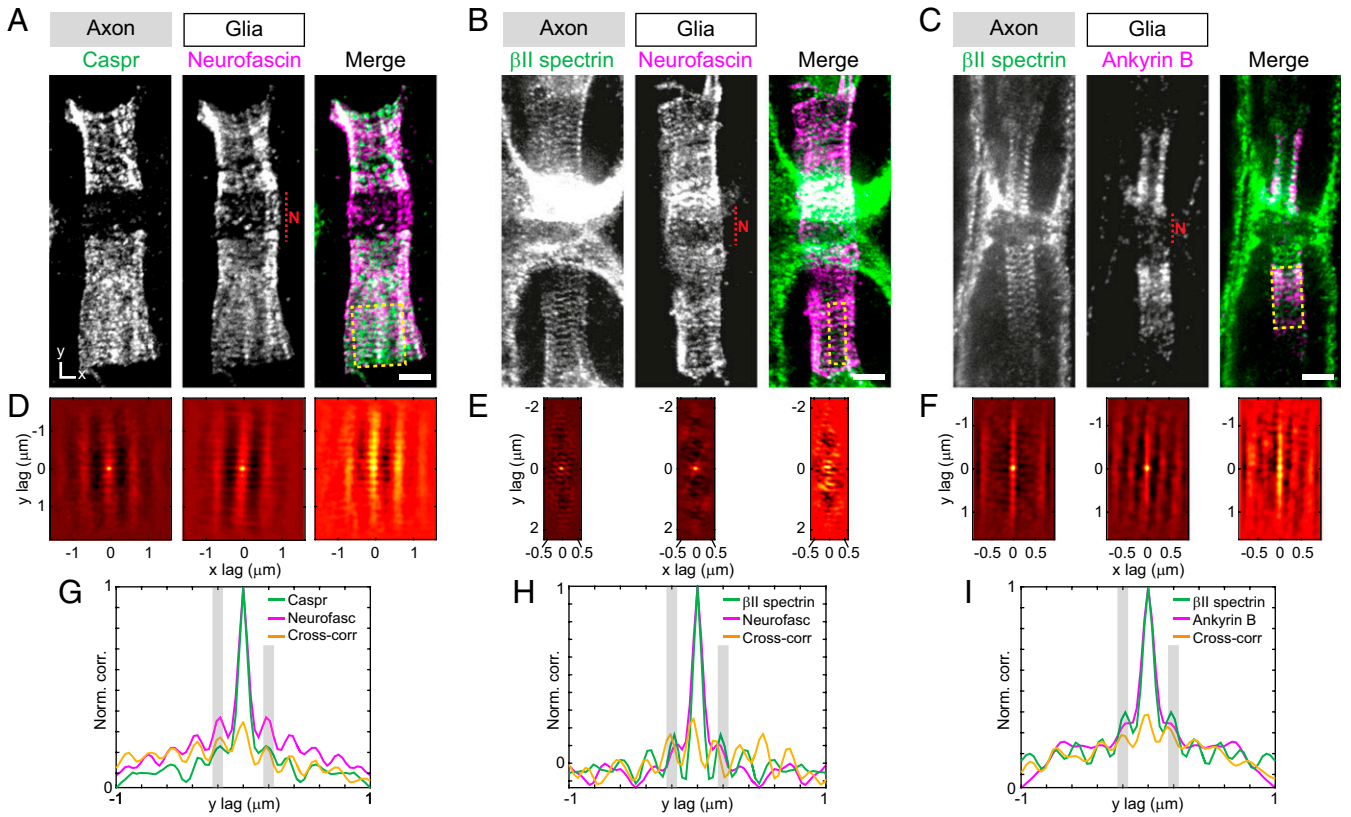

Fig. 4. Nanoscale alignment of the axonal and glial cytoskeleton at paranodes. Two-color STED images of paranodes labeled for (*A*) axonal Caspr and glial neurofascin, (*B*) axonal betaII spectrin and glial neurofascin, and (*C*) axonal betaII spectrin and glial ankyrin B (polyclonal antibody). Single-color images and overlays are shown. The red dashed line indicates the position of the node ("N"). (*D–F*) AC (for single-channel images) and cross-correlation (CC, for the merged image) of the regions indicated by the yellow dashed boxes in *A–C*. The *y* axis is aligned with the axon. A longitudinal periodicity can be observed for all AC and CC. (*G–I*) Vertical line profile of intensities along the panels shown in *D*, *E*, and *F*, respectively. The gray bars highlight the ±0.2 μm *y* lag. All proteins show peaks at the expected position, and CC indicates in-phase colocalization (*G* and *I*) or a slight phase shift (*H*). All image data were smoothed with a 1-pixel low-pass Gaussian filter and represent the overlay of several optical sections. (All scale bars, 1 μm.)

crovilli (7, 38). Investigations of the nodes in the CNS could hence provide different results and clarify the mechanisms that lead to the fine positioning of adhesion proteins and channels at nodal gaps. Furthermore, analysis of heminodes (the structures at the edges of neighboring myelinating cells that eventually fuse into complete nodes) at the nanoscale during the myelination process may clarify the mechanisms of the axon–glia interplay.

The organization of channels at nodal gaps is particularly intriguing, with the $K_v7.2$ subunit showing a much higher order compared with the interleaved Na_v channels. Impairment in Na_v channel expression results in delayed maturation of the nodes of Ranvier and slows down nerve conduction velocity (39, 40), whereas mutations in nodal potassium channels are associated with myokymia, epilepsies, and encephalopathies (41, 42). The mechanisms leading to the accumulation of Na_v channels at the nodes in the PNS are dependent on neurofascin-186 and NrCAM (15). However, it is poorly understood how $K_v7.2$, which has an ankyrin G binding site, is recruited at the nodes. Clustering of $K_v7.2$ (but not Na_v channels) at the nodes is abolished in *quivering-3J* mice, which lack the betaIV spectrin C terminus, even if these two proteins do not interact (43). This evidence, along with the presented data, might suggest the presence of different mechanisms for the clustering and/or organization of sodium and potassium channels at the nodes.

Nanoscopy of the nodes revealed a frequent asymmetry and inhomogeneity in the organization of the nodal proteins, with different lattice geometries on opposing sides, including lines and/or furrows. This latter feature was predominantly observed for Na_v channels, and other markers, like $K_v7.2$ and neurofascin, concomitantly showed similar distributions (Fig. S4). To understand the function of this spatial organization, several points will need clarification: (*i*) whether it is an artifact introduced by the sample preparation, even if this was observed with different fixation and permeabilization procedures; (*ii*) whether all nodes feature this inhomogeneity and whether it appears only on one particular side of the node; (*iii*) whether this structure is present already at heminodes, or if it appears merely in mature nodes; and (*iv*) whether the glia has an influence in creating the nodal asymmetry. Further experiments are therefore required to understand the origin and meaning of this morphological disparity.

The discovery of the actin/spectrin subcortical periodicity at internodes and in oligodendrocyte precursors already suggested the presence of a periodic organization of the cytoskeleton at paranodes (5, 6). At the same time, it has been shown that the glial cytoskeleton undergoes severe rearrangements during the ensheathment process and, in particular, that F-actin disassembly is a critical step at this stage (10, 11). Despite the periodic organization in myelinating precursors (5, 6), betaII spectrin is not present at myelin loops, whereas ankyrin B is still expressed and seems to be the main component of the subcortical cytoskeleton. Ankyrin B interacts with the adhesion protein neurofascin-155, but its targeting to paranodes follows independent mechanisms (23). Therefore, it is not clear how the glial cytoskeleton regulates the positioning of the adhesion molecule neurofascin-155 to permit the axon–glia alignment. The positioning of actin bundles at the paranodal loops is also not clear, as they intercalate with

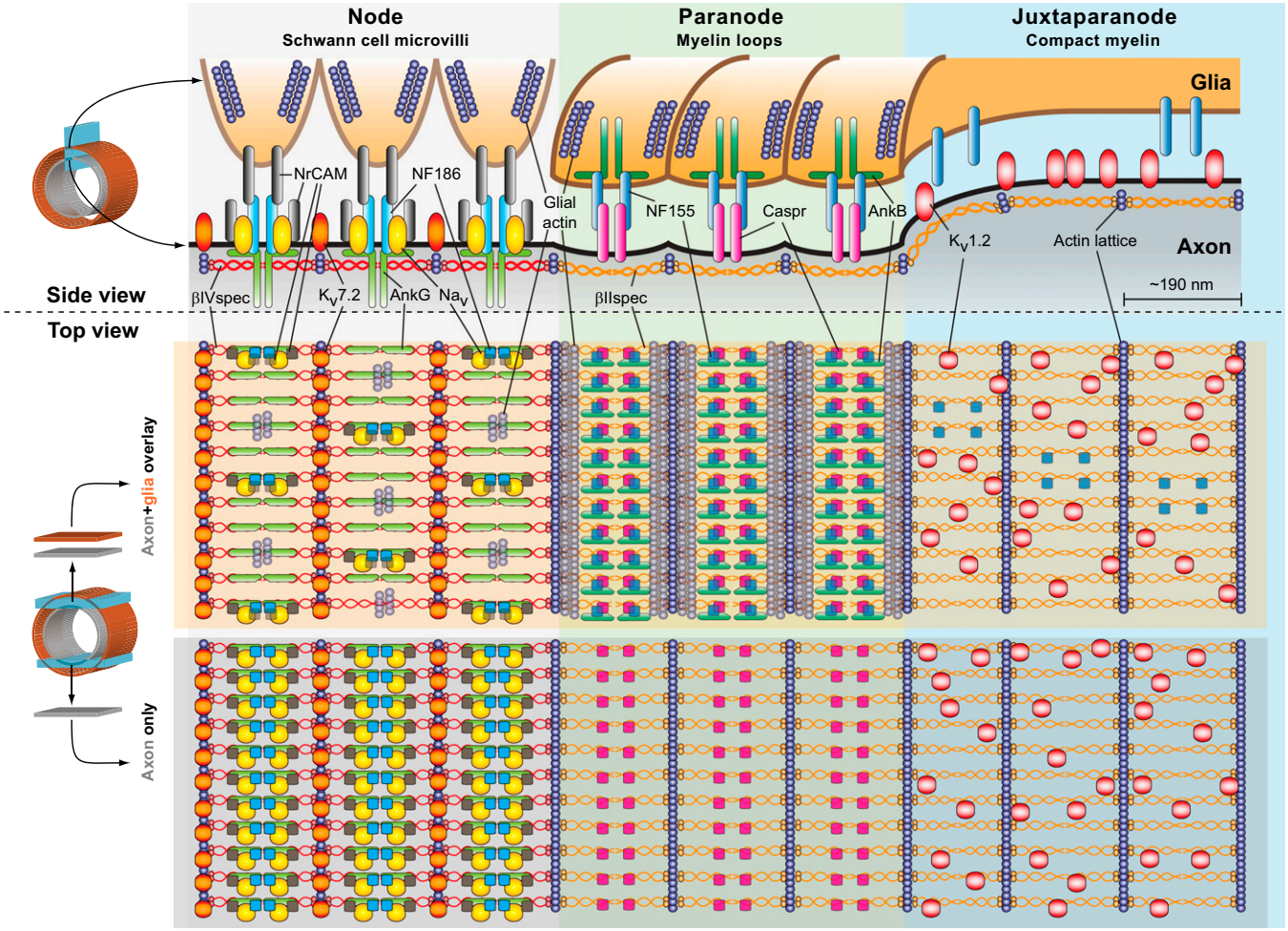

Fig. 5. Proposed model for the molecular organization of nodes of Ranvier in the PNS. The molecular organization of each different compartment (node, paranode, and juxtaparanode) is displayed to highlight both the vertical (*Upper*, side view) and the lateral (*Lower*, top view) positioning of the glial and axonal cytoskeleton. The upper part of the top view is an overlay of the axonal and glial proteins and highlights the influence of the glia on the organization of the nodal gaps. The lower part shows the organization of the axonal components only, without the influence of the glia. Actin and spectrin (and ankyrin G at the nodal gap) constitute a continuous ∼190-nm periodic axonal subcortical scaffold onto which the other components (channels and adhesion molecules) assemble at discrete positions possibly because of the interplay with the glia. At nodes, these components can feature a 2D hexagonal-like periodic organization, also characteristic of proteins present in the microvilli (top view, *Upper*), or a one-dimensional longitudinal periodicity (top view, *Lower*). Positioning of nodal $K_v7.2$ follows almost exclusively a one-dimensional order and does not seem to be influenced by the microvilli. At paranodes, glial and axonal proteins show a highly regular one-dimensional periodic organization that probably reflects the position of myelin loops. The glial and axonal cytoskeleton are aligned and the actin/spectrin scaffold might be densely occupied. It appears that actin bundles are positioned at the side of myelin loops as they alternate neurofascin bands. At juxtaparanodes, actin and spectrin are periodically arranged. However, $K_v1.2$ channels do not exhibit a specific pattern but are complementary to neurofascin. AnkB, ankyrin B; AnkG, ankyrin G; βIIspec, betaII spectrin; βIVspec, betaIV spectrin; $K_v1.2$, $K_v1.2$ channels; $K_v7.2$, $K_v7.2$ (KCNQ2); Na_v, Na_v channels; NF155, neurofascin-155; NF186, neurofascin-186.

neurofascin-155 and hence the PNJ (Fig. 3), and the structure they form appears different from the fine and thin actin filaments composing the subcortical lattice in the axons. Possibly, these actin bundles are positioned on the edges of the myelin loops (Fig. 5). Elucidating the mechanisms and timing of the rearrangement of the actin/spectrin/ankyrin scaffold during myelination will therefore be crucial to comprehend the process leading to the formation of paranodes.

Ankyrins bind to spectrin, sodium channels, and adhesion molecules, thereby connecting the subcortical actin/spectrin cytoskeleton to the extracellular environment. Depletion of ankyrin G leads to the loss of the entire AIS structure, underscoring the importance of ankyrins as scaffolding proteins (44). However, no ankyrin isoforms are reported on the axonal side of paranodes (23), and at the same time, PNJs are found to be intact in mice lacking axonal betaII spectrin (45). Nevertheless, the presented data show a strong correlation between the position of the periodic betaII spectrin subcortical cytoskeleton and the PNJ (Fig. 5), suggesting the presence of other proteins that exert the anchoring function of ankyrin. Protein 4.1B is a possible candidate (46), and therefore, the ultrastructural molecular organization of 4.1B might be the missing link between the positioning of the PNJ and the axonal cytoskeleton.

The fact that all of the proteins analyzed exhibit a quasi–one-dimensional organization at paranodes may indicate that the majority of the docking sites on the actin/spectrin subcortical axonal lattice are actually occupied (Fig. 5), making the axon–glia interaction very tight. Unfortunately, the labeling strategy (using antibodies) and imaging technique used in this study do not currently provide sufficient resolution to identify the presence of subpatterns along the Caspr and neurofascin-155 paranodal bands. Therefore, it is not possible, at present, to establish a relationship between the ∼190-nm periodic pattern formed by the

Table 1. List of proteins analyzed in the present study, along with their function, position at the nodes, localization, reagents used for the detection, fixation, and permeabilization conditions (Fig. S1*A*)

Protein	Function	Compartment	Location	Label	Fixation/permeabilization
βIV spectrin	Cytoskeleton	Nodal gap	Axon	Anti-βIV spectrin SD	Methanol/–*
Ankyrin G	Cytoskeleton	Nodal gap	Axon	Santa Cruz, Sc-28561	PFA 4%/methanol
				Santa Cruz, Sc-12719	PFA 4%/methanol
Na_v channels	Ion channel	Nodal gap	Axon	Sigma-Aldrich, S8809	PFA 4% + Triton 0.1%/Triton 0.5%*
K_v7.2 (KCNQ2)	Ion channel	Nodal gap	Axon	Synaptic Systems, 368 003	PFA 4%/methanol
				Abcam, Ab22897	PFA 4%/methanol
Neurofascin-186	CAM	Nodal gap	Axon	Abcam, Ab31457	PFA 4%/methanol
NrCAM	CAM	Nodal gap	Axon and glia	Abcam, Ab24344	PFA 4%/methanol
Actin	Cytoskeleton	Nodal gap	Axon and glia	Phalloidin	PFA 4%/Triton 0.5%*
		Paranode	Axon and glia		
		Juxtaparanode	Axon		
βII spectrin	Cytoskeleton	Paranode	Axon	BD Bioscience, 612563	PFA 4%/methanol
		Juxtaparanode	Axon		
Ankyrin B	Cytoskeleton	Paranode	Glia	NeuroMab, 73–145	PFA 4%/methanol
				Santa Cruz, Sc-28560	
Neurofascin-155	CAM	Paranode	Glia	Abcam, Ab31457	PFA 4%/methanol
Caspr	CAM	Paranode	Axon	NeuroMab, 75–001	PFA 4%/methanol
K_v1.2	Ion channel	Juxtaparanode	Axon	NeuroMab, 73–008	PFA 4%/methanol
Acetylated tubulin	Cytoskeleton		Axon	Sigma-Aldrich, T7451	PFA 4%/methanol

A dash (–) indicates no further permeabilization performed.
*The fixation and permeabilization conditions used for two-color stainings.

adhesion molecules and the transverse bands spaced by ∼30 nm, as evident from electron microscopy studies at the PNJ (13, 22).

The potassium channels K_v1.2 do not exhibit a periodic organization at juxtaparanodes, even if the regular spectrin/actin scaffold is present (5), whereas in mice lacking axonal betaII spectrin, K_v channels were found to invade paranodes (45). This result can be explained in two ways: (*i*) the identification of a lattice at juxtaparanodes is technically difficult due to the fine 3D structure of the compartment and the presence of channels and membrane folds, and (*ii*) the interaction between axon and glia does not induce a periodic docking of transmembrane proteins onto the actin/spectrin scaffold at juxtaparanodes (Fig. 5). Analysis of other transmembrane and adaptor proteins of axon and glia enriched at juxtaparanodes and internodes will be necessary to appreciate the organization of proteins underneath compact myelin more fully.

In conclusion, we investigated and presented the nanoscale molecular organization of 12 proteins at the nodes of Ranvier of sciatic nerve fibers, providing a superresolution map of this compartment. Therefore, the presented results pave the way for further studies that will be required for a deeper characterization of these structures. Our work notably highlights the importance of the 2D organization of molecules at nodes, a yet-unexplored aspect, and provides evidence of the axon–glia interplay in their organization. Although a tight longitudinal periodic alignment of the glial and axonal cytoskeleton is present at paranodes, at nodal gaps the organization can be a complex lattice whose arrangement is influenced by the glial microvilli. Nodes are the largest known vertebrate intercellular junctions, and their ultrastructural molecular organization is strikingly tidy and coordinated. It is likely that (autoimmune) neurodegenerative and demyelinating diseases, besides altering the structure of the PNJs (34), affect their nanoscale molecular order. We are convinced that further insights regarding the pathogenic mechanisms of these diseases will come from the study of the ultrastructural anatomy of nodes of Ranvier in animal models or explants from patients.

Materials and Methods

Sciatic nerves were extracted from C57BL/6 mice 3–6 mo old (mixed sexes) in accordance with Animal Welfare Law of the Federal Republic of Germany (Tierschutzgesetz der Bundesrepublik Deutschland, TierSchG) and the regulation about animals used in experiments (August 1, 2013, Tierschutzversuchsverordnung). For the procedure of euthanizing rodents for subsequent preparation of any tissue, all regulations given in §4 TierSchG are followed. Because euthanization of animals is not an experiment on animals according to §7 Abs. 2 Satz 3 TierSchG, no specific authorization or notification is required. Nerves were fixed and permeabilized differently depending on the antibody staining (Table 1 and Fig. S1*A*). When possible, effective labeling and preservation of the structures of interest were first tested on hippocampal neurons in comparable conditions. Free-floating partially teased fibers were blocked in PBS containing 1% BSA for 45 min. Both primary and secondary antibody incubations were performed for 1–2 h at room temperature or overnight at 4 °C in PBS supplemented with 0.05% Triton X-100. After each step, samples were rinsed three times for 10 min in PBS with 0.05% Triton X-100. At the end, samples were completely teased on a coverslip and mounted in Mowiol supplemented with DABCO.

The proteins and corresponding antibodies used in the present study are listed in Table 1. Anti-betaIV spectrin SD antibody was a kind gift of Michele Solimena, Dresden University of Technology, Dresden, Germany. Secondary antibodies (sheep anti-mouse, Dianova, cat. no. 515–005-003; goat–anti-rabbit, Dianova, cat. no. 111–005-003) were labeled with STAR580 (Abberior, cat. no. 1–0101-005-2) or STAR635P (Abberior, cat. no. 1–0101-007-6). Phalloidin was coupled to STAR635 (Abberior, cat. no. 2–0205-002-5).

Imaging was performed on a two-color Abberior STED 775 QUAD scanning microscope (Abberior Instruments GmbH) equipped with 488 nm, 561 nm, and 640 nm pulsed excitation lasers; a pulsed 775 nm STED laser; and a 100× oil immersion objective lens (N.A. 1.4). Pixel size was 30 nm for all of the images. Stacks were acquired by using the Abberior easy3D STED module. Laser powers and dwell times were optimized for each sample.

All acquired images were processed and visualized using the ImSpector software package (Max-Planck Innovation) and ImageJ (https://imagej.nih.gov/ij/). Smoothing was performed using a 1-pixel low-pass Gaussian filter within the software ImSpector. Brightness and contrast were applied uniformly to all parts of the images. Line profiles were measured along a 3-pixel wide line. Interpeak distances were determined using the multipeak fitting function in OriginPro8.5.

AC and cross-correlation analyses were performed for one- and two-color images, respectively. Regions of interest (e.g., nodes, paranodes) were cropped and rotated, to align the vertical axis of the correlation with the axon orientation, maintaining the pixel size. The correlations were calculated with the Matlab R2015b function "xcorr2," subtracting beforehand the average of the image, to avoid an (uninformative) additive triangular signal in the correlation. The profile along the vertical axis of the correlation image was examined for periodicities.

ACKNOWLEDGMENTS. We acknowledge Michele Solimena for the betaIV spectrin SD antibody. We thank Dr. Grazvydas Lukinavicius and Dr. Steffen J. Sahl (MPI-BPC, Göttingen) for critical readings of the manuscript and discussion. This work was supported through the Center for Nanoscale Microscopy and Molecular Physiology of the Brain (CNMPB) in Göttingen.

1. Xu K, Zhong G, Zhuang X (2013) Actin, spectrin, and associated proteins form a periodic cytoskeletal structure in axons. *Science* 339(6118):452–456.
2. Zhong G, et al. (2014) Developmental mechanism of the periodic membrane skeleton in axons. *eLife* 3:3.
3. D'Este E, Kamin D, Göttfert F, El-Hady A, Hell SW (2015) STED nanoscopy reveals the ubiquity of subcortical cytoskeleton periodicity in living neurons. *Cell Reports* 10(8): 1246–1251.
4. Leterrier C, et al. (2015) Nanoscale architecture of the axon initial segment reveals an organized and robust scaffold. *Cell Reports* 13(12):2781–2793.
5. D'Este E, et al. (2016) Subcortical cytoskeleton periodicity throughout the nervous system. *Sci Rep* 6:22741.
6. He J, et al. (2016) Prevalent presence of periodic actin-spectrin-based membrane skeleton in a broad range of neuronal cell types and animal species. *Proc Natl Acad Sci USA* 113(21):6029–6034.
7. Eshed-Eisenbach Y, Peles E (2013) The making of a node: A co-production of neurons and glia. *Curr Opin Neurobiol* 23(6):1049–1056.
8. Zhang C, Rasband MN (2016) Cytoskeletal control of axon domain assembly and function. *Curr Opin Neurobiol* 39:116–121.
9. Poliak S, Peles E (2003) The local differentiation of myelinated axons at nodes of Ranvier. *Nat Rev Neurosci* 4(12):968–980.
10. Nawaz S, et al. (2015) Actin filament turnover drives leading edge growth during myelin sheath formation in the central nervous system. *Dev Cell* 34(2):139–151.
11. Zuchero JB, et al. (2015) CNS myelin wrapping is driven by actin disassembly. *Dev Cell* 34(2):152–167.
12. Ichimura T, Ellisman MH (1991) Three-dimensional fine structure of cytoskeletal-membrane interactions at nodes of Ranvier. *J Neurocytol* 20(8):667–681.
13. Schnapp B, Peracchia C, Mugnaini E (1976) The paranodal axo-glial junction in the central nervous system studied with thin sections and freeze-fracture. *Neuroscience* 1(3):181–190.
14. Eshed Y, et al. (2005) Gliomedin mediates Schwann cell-axon interaction and the molecular assembly of the nodes of Ranvier. *Neuron* 47(2):215–229.
15. Feinberg K, et al. (2010) A glial signal consisting of gliomedin and NrCAM clusters axonal Na+ channels during the formation of nodes of Ranvier. *Neuron* 65(4): 490–502.
16. Occhi S, et al. (2005) Both laminin and Schwann cell dystroglycan are necessary for proper clustering of sodium channels at nodes of Ranvier. *J Neurosci* 25(41):9418–9427.
17. Saito F, et al. (2003) Unique role of dystroglycan in peripheral nerve myelination, nodal structure, and sodium channel stabilization. *Neuron* 38(5):747–758.
18. Devaux JJ, Kleopa KA, Cooper EC, Scherer SS (2004) KCNQ2 is a nodal K+ channel. *J Neurosci* 24(5):1236–1244.
19. Pan Z, et al. (2006) A common ankyrin-G-based mechanism retains KCNQ and NaV channels at electrically active domains of the axon. *J Neurosci* 26(10):2599–2613.
20. Tait S, et al. (2000) An oligodendrocyte cell adhesion molecule at the site of assembly of the paranodal axo-glial junction. *J Cell Biol* 150(3):657–666.
21. Melendez-Vasquez CV, et al. (2001) Nodes of Ranvier form in association with ezrin-radixin-moesin (ERM)-positive Schwann cell processes. *Proc Natl Acad Sci USA* 98(3):1235–1240.
22. Nans A, Einheber S, Salzer JL, Stokes DL (2011) Electron tomography of paranodal septate-like junctions and the associated axonal and glial cytoskeletons in the central nervous system. *J Neurosci Res* 89(3):310–319.
23. Chang KJ, et al. (2014) Glial ankyrins facilitate paranodal axoglial junction assembly. *Nat Neurosci* 17(12):1673–1681.
24. Charles P, et al. (2002) Neurofascin is a glial receptor for the paranodin/Caspr-contactin axonal complex at the axoglial junction. *Curr Biol* 12(3):217–220.
25. Gollan L, Salomon D, Salzer JL, Peles E (2003) Caspr regulates the processing of contactin and inhibits its binding to neurofascin. *J Cell Biol* 163(6):1213–1218.
26. Pillai AM, et al. (2009) Spatiotemporal ablation of myelinating glia-specific neurofascin (Nfasc NF155) in mice reveals gradual loss of paranodal axoglial junctions and concomitant disorganization of axonal domains. *J Neurosci Res* 87(8):1773–1793.
27. Sun XY, et al. (2009) A novel Caspr mutation causes the shambling mouse phenotype by disrupting axoglial interactions of myelinated nerves. *J Neuropathol Exp Neurol* 68(11):1207–1218.
28. Byers TJ, Branton D (1985) Visualization of the protein associations in the erythrocyte membrane skeleton. *Proc Natl Acad Sci USA* 82(18):6153–6157.
29. Rasband MN, Trimmer JS, Peles E, Levinson SR, Shrager P (1999) K+ channel distribution and clustering in developing and hypomyelinated axons of the optic nerve. *J Neurocytol* 28(4-5):319–331.
30. Rasband MN, et al. (1998) Potassium channel distribution, clustering, and function in remyelinating rat axons. *J Neurosci* 18(1):36–47.
31. Pedraza L, Huang JK, Colman DR (2001) Organizing principles of the axoglial apparatus. *Neuron* 30(2):335–344.
32. Rasband MN (2004) It's "juxta" potassium channel! *J Neurosci Res* 76(6):749–757.
33. Stathopoulos P, Alexopoulos H, Dalakas MC (2015) Autoimmune antigenic targets at the node of Ranvier in demyelinating disorders. *Nat Rev Neurol* 11(3):143–156.
34. Arancibia-Carcamo IL, Attwell D (2014) The node of Ranvier in CNS pathology. *Acta Neuropathol* 128(2):161–175.
35. Buttermore ED, Thaxton CL, Bhat MA (2013) Organization and maintenance of molecular domains in myelinated axons. *J Neurosci Res* 91(5):603–622.
36. Faivre-Sarrailh C, Devaux JJ (2013) Neuro-glial interactions at the nodes of Ranvier: Implication in health and diseases. *Front Cell Neurosci* 7:196.
37. Raine CS (1984) On the association between perinodal astrocytic processes and the node of Ranvier in the C.N.S. *J Neurocytol* 13(1):21–27.
38. Susuki K, et al. (2013) Three mechanisms assemble central nervous system nodes of Ranvier. *Neuron* 78(3):469–482.
39. Kearney JA, et al. (2002) Molecular and pathological effects of a modifier gene on deficiency of the sodium channel Scn8a (Na(v)1.6). *Hum Mol Genet* 11(22):2765–2775.
40. Eijkelkamp N, et al. (2012) Neurological perspectives on voltage-gated sodium channels. *Brain* 135(Pt 9):2585–2612.
41. Greene DL, Hoshi N (September 19, 2016) Modulation of Kv7 channels and excitability in the brain. *Cell Mol Life Sci*, 10.1007/s00018-016-2359-y.
42. Cooper EC (2011) Made for "anchorin": Kv7.2/7.3 (KCNQ2/KCNQ3) channels and the modulation of neuronal excitability in vertebrate axons. *Semin Cell Dev Biol* 22(2):185–192.
43. Devaux JJ (2010) The C-terminal domain of βIV-spectrin is crucial for KCNQ2 aggregation and excitability at nodes of Ranvier. *J Physiol* 588(Pt 23):4719–4730.
44. Hedstrom KL, Ogawa Y, Rasband MN (2008) AnkyrinG is required for maintenance of the axon initial segment and neuronal polarity. *J Cell Biol* 183(4):635–640.
45. Zhang C, Susuki K, Zollinger DR, Dupree JL, Rasband MN (2013) Membrane domain organization of myelinated axons requires βII spectrin. *J Cell Biol* 203(3):437–443.
46. Denisenko-Nehrbass N, et al. (2003) Protein 4.1B associates with both Caspr/paranodin and Caspr2 at paranodes and juxtaparanodes of myelinated fibres. *Eur J Neurosci* 17(2):411–416.